LITHOS 424-425 (2022) 106759

Contents lists available at ScienceDirect

LITHOS

journal homepage: www.elsevier.com/locate/lithos

Thermal history and parental magma composition of early olivine gabbros of the Troodos ophiolite, Cyprus

Wen-Jun Hu [a], Mei-Fu Zhou [a,b,*], John Malpas [c], Zhenchao Wang [b]

[a] School of Earth Resources, China University of Geosciences, Wuhan, China
[b] State Key Laboratory of Ore Deposit Geochemistry, Institute of Geochemistry, Chinese Academy of Sciences, Guiyang 550081, China
[c] Department of Earth Sciences, The University of Hong Kong, Hong Kong, China

ARTICLE INFO

Keywords:
Troodos ophiolite
Olivine gabbros
Melt-rock reaction
Parental magma

ABSTRACT

Samples of an early olivine gabbro in the lower plutonic sequence of the Troodos ophiolite were studied to constrain their thermal history and the compositions of their parental magma. These rocks exhibit typical orthocumulate textures and petrographic evidence of reaction between a migrating interstitial magma and a crystal mush, including embayed margins of olivine crystals and irregular ragged grain boundaries of clinopyroxenes, indicating dissolution of olivine and crystallization of clinopyroxene, followed by crystallization of plagioclase within the framework of olivine and clinopyroxene. All the minerals exhibit relatively homogeneous compositions, without any clear zoning in either their major or trace elements, indicating that the minerals and migrating magma reached equilibrium. The rare earth element (REE) distribution between clinopyroxene and plagioclase records an equilibrium temperature of about 1300 °C, but the Mg-exchange geothermometer yielded a lower temperature of about 1000 °C. These different closure temperatures indicate a rapid cooling history with a cooling rate of −2 °C/year log units. The low TiO_2 contents and additional trace element compositions of clinopyroxene show that the parental magma of the gabbro was related to boninitic magmas of the ophiolite. Consequently, we show that some boninitic lavas in the upper oceanic crust have been affected by melt-rock reaction process during their ascent through the lower crust, and therefore their composition cannot be directly used to constrain the composition of the primary boninites.

1. Introduction

The igneous oceanic crust consists of an upper part including extrusive lavas and the dykes that feed them (White and Klein, 2014), and a lower part made up of different types of plutonic rock, e.g., gabbros, troctolite and wehrlite (Coogan, 2014). This structure results from a magma plumbing system that operates during the formation of the oceanic lithosphere (White, 2013). At a spreading center, magmas are extracted from the upwelling mantle and ponded in magma chambers. Crystallization of magmas in the chambers produces the lower oceanic crust (Coogan, 2014), whereas the remaining melt fraction after partial crystallization is injected as sills or dikes or erupted as lavas (Sinton and Detrick, 1992). The lower oceanic crust thus preserves critical information about the nature and evolution of magmas before subsequent eruption to the surface (Coogan, 2014).

To understand the possible links between the lower plutonic rocks and the upper lavas, it is imperative to constrain the compositions of the parental magmas of the plutonic rocks. Bulk compositions of the plutonic rocks may be used to estimate the nature of their parental magmas, but this requires large-scale systematic sampling, and can lead to imprecise results because the plutonic rocks do not equate to the liquids from which they formed (Bowen, 1928; Niu et al., 2002; Wager and Brown, 1968), and the plutonic rocks could have developed by fractionation in an open system (e.g., Coogan et al., 2000; Lissenberg et al., 2013; Lissenberg and Dick, 2008; Lissenberg and MacLeod, 2016; Sanfilippo et al., 2020; Yang et al., 2019; Zhang et al., 2020). Major and trace element compositions of minerals, in conjunction with appropriate distribution coefficients, provide a better way of estimating the magma composition, but mineral compositions can be modified by a series of post-crystallization processes, e.g., interaction with migrating or trapped liquids, and inter/intra- grain diffusion (Barnes, 1986; Borghini and Rampone, 2007; Gao et al., 2007; Godel et al., 2011; Lissenberg et al., 2013; Lissenberg and Dick, 2008; Lissenberg and MacLeod, 2016; Rampone et al., 2016; Sun and Liang, 2014).

* Corresponding author at: School of Earth Resources, China University of Geosciences, Wuhan, China.
E-mail address: zhoumeifu@hotmail.com (M.-F. Zhou).

https://doi.org/10.1016/j.lithos.2022.106759
Received 3 October 2021; Received in revised form 1 June 2022; Accepted 1 June 2022
Available online 7 June 2022

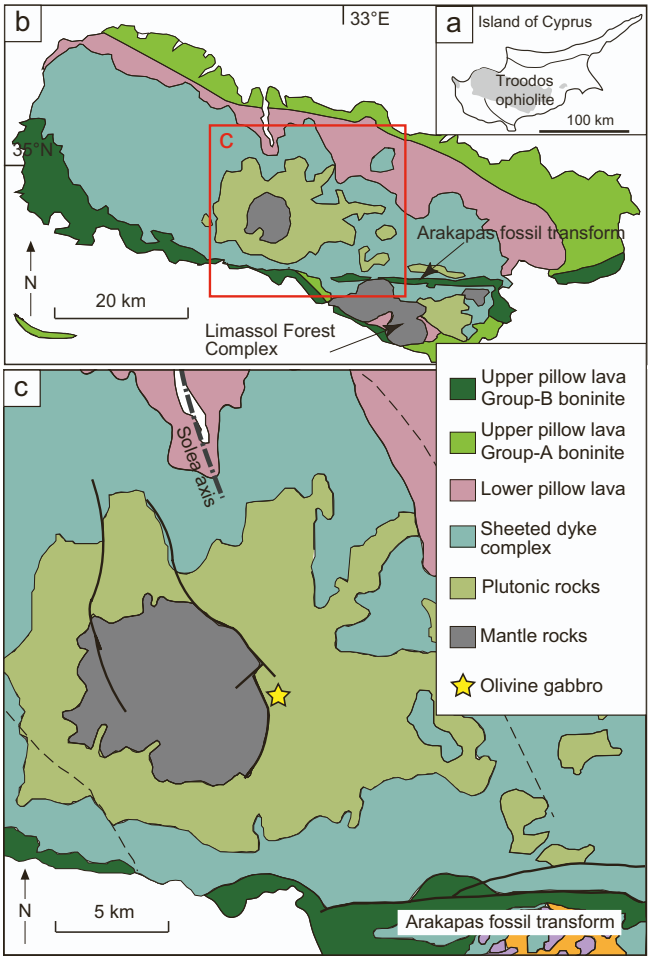

Fig. 1. Simplified map of (a) Cyprus and (b) the Troodos ophiolite (modified after Osozawa et al., 2012) and (c) mantle and gabbro sequence near the Solea graben (modified after Abelson et al., 2001).

Given that in-situ investigation of the lower oceanic crust is difficult due to its relative inaccessibility, ophiolites have been widely used as analogues. Well-developed and well-preserved ophiolite complexes allow for better sampling and direct observation of the relationships between the lower oceanic crust and other associated parts of the lithosphere (Coogan, 2014; Coogan et al., 2003; Liu et al., 2018, 2021; Marchesi et al., 2009; Sanfilippo and Tribuzio, 2013; Wang et al., 2021; Yamasaki et al., 2006). The Troodos ophiolite, one of the most studied ophiolites in the world (Edwards et al., 2010; Miyashiro, 1973; Pearce et al., 1984; Robertson and Xenophontos, 1993), is thought to have formed at a slow-spreading center above a paleo-subduction zone (Abelson et al., 2001; Malpas, 1990; Pearce and Robinson, 2010). Previous studies of plutonic rocks of the Troodos ophiolite, especially the CY-4 drilling project, provided a basic knowledge about the generation of the lower oceanic crust and revealed a complex magma plumbing system (Gibson et al., 1989; Malpas, 1990; Thy, 1987a and 1987b).

To date, the genesis of the Troodos lower oceanic crust and its relationship with the overlying lavas has been examined largely through major element chemistry of whole-rocks and minerals (e.g., Thy, 1987a and 1987b). In this study, we selected olivine gabbros from the lower plutonic section of the Troodos ophiolite close to the mantle/crust boundary (Fig. 1) and measured both the major elements and trace elements of the constituent minerals. Rare earth elements (REE) are of particular interest as they have very slow diffusion coefficients in the major minerals (e.g., clinopyroxene and plagioclase) and hence can largely preserve information about early igneous processes (Lee et al., 2007; Sun and Liang, 2014). Together with microtextures, mineral geothermometers were used to investigate the thermal and crystallization histories of the gabbros. The studied gabbros show clear petrographic evidence of interaction between a migrating magma and a crystal mush; consequently, it is necessary to investigate the effects of this interaction on the melt compositions as crystallization proceeded.

2. Geological background

The Troodos ophiolite in Cyprus consists of the main Olympos (Axis) Sequence and the Arakapas (Transform) Sequence, separated by a possible fossil transform fault (Fig. 1; Gass et al., 1994; Geological Survey Department Cyprus, 1995). The main Olympos (Axis) Sequence is one of the most complete and typical ophiolitic sequences in the world, and includes serpentinized mantle peridotites, plutonic rocks, sheeted-dykes and lavas. The zircon U—Pb ages of plagiogranites scattered amongst the plutonic rocks indicate that the ophiolite was formed at 90–92 Ma (Chen et al., 2020; Mukasa and Ludden, 1987; Osozawa et al., 2012). The Arakapas (Transform) Sequence has a triangular-shaped outcrop pattern bounded to the north by the linear Arakapas Transform Fault (Simonian and Gass, 1978). The rock assemblage here is the same as that of the main Olympos (Axis) Sequence, but structural relationships between lithologies are much more complicated.

Lavas of the Troodos ophiolite have a clear chemostratigraphy (Mehegan, 1988; Pearce and Robinson, 2010; Regelous et al., 2014; Robinson et al., 1983), with a lower pillow lava (LPL) series composed of arc tholeiites, overlain by a boninitic upper pillow lava (UPL) series. The LPL includes three units: a basic-ultrabasic unit (Unit I) overlain by an intermediate-acid Unit (Unit II) and then a basic to basic-intermediate unit (Unit III) (Pearce and Robinson, 2010). The LPL gradually grade downward into the sheeted-dykes through a mixed unit of lavas and dykes named the Basal Group (Geological Survey Department Cyprus, 1995). The UPL contains different types of boninite and boninitic lavas (e.g., Cameron, 1985; Osozawa et al., 2012). In this study, we adopt the classification scheme of Osozawa et al. (2012) that divides the UPL into two groups. The first group is mainly distributed on the northern flank of the main Olympos Sequence, and to a lesser extent locally in the Arakapas Sequence. The second group is mainly found along the Arakapas valley and its western and eastern extensions (Osozawa et al., 2012). This second group of boninites occupies the highest stratigraphic level and were referred to as “infill lavas” by Gass et al. (1994). In the field, the two groups of boninites are mostly overlain by the late Campanian (ca. 75 Ma) Perapedhi Formation. However, one small outcrop of volcanic glass of the second group, that is covered by middle Paleogene to early Miocene sedimentary rocks, yielded an Ar—Ar age of 55.5 ± 0.9 Ma (Osozawa et al., 2012). This single date is a significant outlier and should be treated with caution.

The second group of boninites is more depleted in composition, having lower TiO_2 and trace element concentrations than the first group (Hu et al., 2021; Osozawa et al., 2012). The two groups have similar HREE concentrations but the second group has lower LREE-MREE concentrations than the first group. In chondrite-normalized REE diagrams, the second group displays “spoon-shaped” patterns whereas those of the first group are flat (Fig. 4 in Osozawa et al. (2012)). Accordingly, Osozawa et al. (2012) named the first group simply ‘boninite’ and the second group ‘depleted boninite’. To avoid confusion, in this study we instead refer to the first and second groups as Group-A and Group-B, respectively (Fig. 1).

It is noteworthy that the geochemistry of the lavas provided the first indication that the Troodos ophiolite formed in a subduction-related environment rather than at a mid-ocean-ridge (Miyashiro, 1973; Robinson et al., 1983). More recent studies highlighted similarities in lava associations between the Troodos ophiolite and the Izu–Bonin–Mariana (IBM) forearc system and argued that this ophiolite most likely developed in a forearc setting at the early stage of subduction (Hu et al., 2021; Ishizuka et al., 2014; Pearce and Robinson, 2010; Stern et al., 2012;

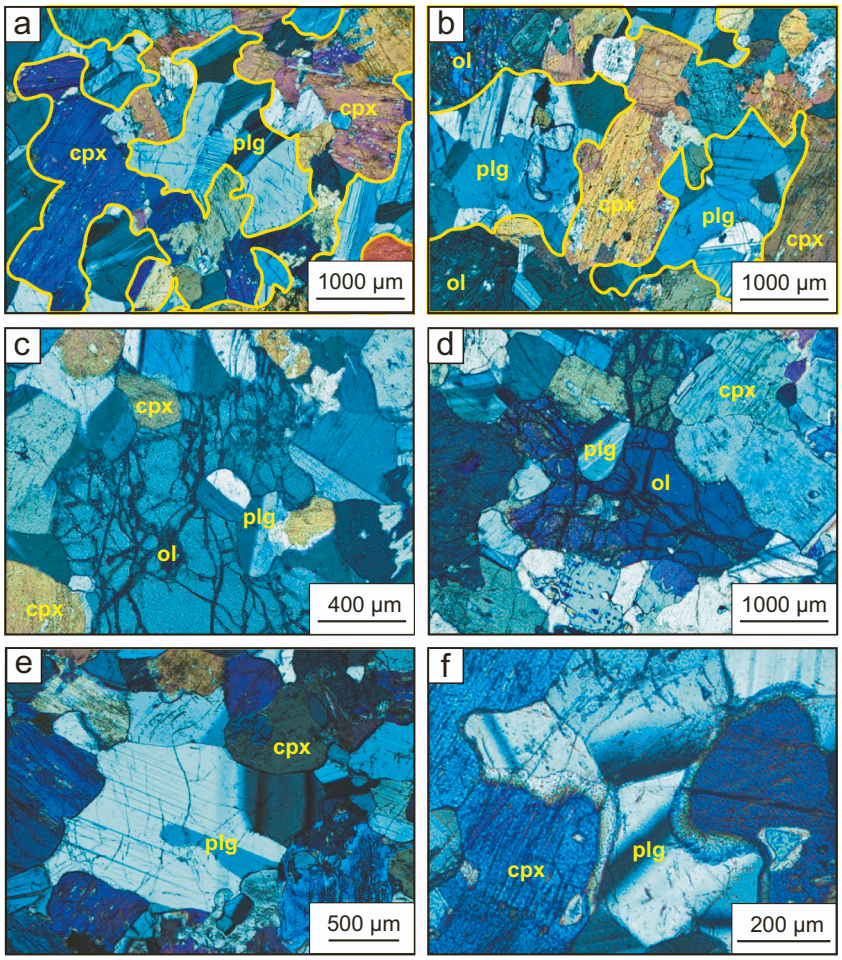

Fig. 2. Microscopic textures of the studied olivine gabbros of the Troodos ophiolite. (a)–(b) orthocumulate texture of olivine gabbros, i.e., early crystallized olivine and clinopyroxene formed a framework that was filled later by plagioclase. (c)–(d) embayed olivine partly replaced secondary plagioclase during its interaction with a later melt. (e)–(f) Deformation twins of plagioclase grains, indicative of compaction of cumulate piles. ol-olivine, cpx-clinopyroxene, opx-orthopyroxene, plg-plagioclase.

Table 1
Major and trace element compositions of olivines of olivine gabbros in the Troodos ophiolite.

Sample No.	CY1706a1	CY1706a2	CY1706b1	CY1706b2	CY1706c
Major element (wt%)					
SiO_2	39.69	39.76	39.11	39.13	40.05
FeO	15.93	15.80	17.08	16.98	15.79
MnO	0.22	0.22	0.23	0.22	0.21
MgO	43.61	43.74	42.25	42.28	43.61
NiO	0.13	0.13	0.16	0.18	0.13
Total	99.59	99.65	98.82	98.79	99.78
Fo	83.0	83.2	81.5	81.6	83.1
Trace element (ppm)					
Sc	4.39	4.22	4.04	3.89	4.30
Ti	30.1	26.6	24.3	28.4	25.5
V	2.94	2.83	2.64	2.97	2.60
Cr	28.0	26.8	27.5	26.2	24.2
Mn	1789	1798	1859	1861	1797
Co	193	194	200	200	196
Ni	1279	1276	1467	1469	1274
Zn	99.2	98.5	80.8	80.7	100

Whattam and Stern, 2011).

The Troodos main Olympus plutonic sequence is also divided into two series, namely an older series of variably deformed plutonic rocks which are intruded by a younger series of undeformed plutonic rocks (Malpas, 1990; Malpas et al., 1989). Both are represented in the CY-4 drill hole of the Cyprus Crustal Study Project, where the younger series occurs deeper in the stratigraphy and intrudes older plutonic rocks emplaced at a shallower level (Thy, 1987a). This stratigraphic relationship is clear only in the drill core and cannot be established in the field where rocks of both series occur throughout the plutonic sequence. The two series also show considerable differences in terms of petrography and geochemistry. The older series comprise gabbros and gabbronorites with typical adcumulate textures (Malpas et al., 1989). They are more evolved in terms of geochemistry with high Ti/Al clinopyroxene and, in the drill core, display three cryptic geochemical reversals together with intermittent normal fractionation intervals (Thy, 1987a). These petrographic and geochemical characteristics suggest that the older series was generated in multiple open system chambers with frequent magma replenishment. The younger intrusions, however, usually display orthocumulate or heteroadcumulate textures (Malpas et al., 1989), and exhibit limited geochemical reversals and low Ti/Al clinopyroxene, suggesting that the gabbros were generated in a more closed system, possibly an off-axis, slow-spreading tectonic environment (Thy, 1987a). Regarding the compositional similarities between lavas and plutonic rocks, it was proposed that the LPL and older plutons are genetically related, whereas the UPL relate to the younger plutons (Thy, 1987a). In this study, we focus on rocks of the younger plutons and their relationships with the UPL.

3. Petrography

Olivine gabbros from the lower part of the plutonic sequence were sampled in this study. They are considered to be representative of the younger series of plutons and are coarse- to medium-grained with typical orthocumulate textures in which intercumulus plagioclase fills spaces between olivine and clinopyroxene cumulate crystals (Fig. 2a and

Table 2
Major and trace element composition of clinopyroxene of olivine gabbros in the Troodos ophiolite.

Sample No.	CY1706a1	CY1706a2	CY1706b1	CY1706b2	CY1706c
Major element (wt%)					
SiO_2	53.21	53.30	52.73	52.73	53.37
TiO_2*	0.19	0.17	0.16	0.16	0.18
Al_2O_3	2.08	2.08	1.85	1.89	2.22
Cr_2O_3	0.40	0.43	0.37	0.42	0.46
FeO	4.36	4.39	4.92	5.07	4.43
MnO	0.14	0.11	0.15	0.13	0.15
MgO	16.61	16.93	17.08	17.56	16.73
CaO	22.36	22.20	21.17	20.44	22.19
Na_2O	0.20	0.18	0.16	0.18	0.17
NiO	0.02	0.02	0.03	0.03	0.01
Total	99.56	99.82	98.61	98.61	99.91
Mg#	87.2	87.3	86.1	86.1	87.1
Trace element (ppm)					
Sc	96.4	90.8	82.5	77.8	95.2
Ti	1118	998	961	963	1084
V	269	252	253	274	267
Cr	3181	3335	2485	2238	3488
Mn	1187	1162	1219	1199	1154
Co	35.1	37.6	38.0	36.9	35.8
Ni	181	194	224	212	187
Zn	22.6	23.6	19.5	18.3	21.8
Sr	4.33	4.28	4.09	3.76	4.29
Y	5.71	5.62	6.15	5.03	5.63
Zr	1.62	1.73	1.74	1.58	1.52
La	0.06	0.07	0.06	0.05	0.05
Ce	0.29	0.28	0.30	0.25	0.27
Pr	0.08	0.07	0.07	0.06	0.07
Nd	0.46	0.48	0.49	0.42	0.46
Sm	0.36	0.35	0.38	0.31	0.35
Eu	0.17	0.16	0.17	0.14	0.16
Gd	0.69	0.69	0.72	0.60	0.69
Tb	0.14	0.14	0.15	0.12	0.14
Dy	1.01	1.04	1.11	0.92	1.03
Ho	0.23	0.22	0.25	0.21	0.23
Er	0.68	0.67	0.72	0.59	0.68
Tm	0.10	0.10	0.11	0.08	0.09
Yb	0.66	0.62	0.71	0.56	0.64
Lu	0.09	0.09	0.10	0.08	0.09

* Contents of TiO_2 of clinopyroxene were determined by LA-ICP-MS

b). The olivine grains are large (>1 mm), anhedral crystals that make up 5–10 modal %. The embayed morphology of the olivine indicates interaction with a later melt after olivine crystallization (Fig. 2c and d). Some domains of olivine grains cut by plagioclase have the same optical orientation. Clinopyroxene commonly occurs as euhedral crystals, most of which are granular to tabular in shape (0.5–1 mm × 1–2 mm), but many grains display complex intergrowths and ragged grain boundaries, indicating formation of new crystals during reaction with melts (Lissenberg and MacLeod, 2016) (Fig. 2a and b). As the only intercumulus phase, plagioclase makes up 20–30 modal%, and occurs as anhedral grains that are largely controlled by the spaces between the cumulus minerals (Fig. 2a and b). The petrography features indicate reaction between a crystal mush and a migrating magma, which led to dissolution of olivine and crystallization of clinopyroxene, followed by crystallization of plagioclase from evolved intergranular melts within the framework of olivine and clinopyroxene. Some plagioclase grains show deformation twins, indicative of compaction of cumulate piles (Zhang et al., 2020) (Fig. 2e and f). No common accessory minerals, such as Fe—Ti oxide and apatite, have been identified in thin sections, suggesting that the evovled intergranular melt were expelled from the cumulate pile during fractionation and compaction.

4. Analytical methods

Mineral major element compositions were determined with a Link

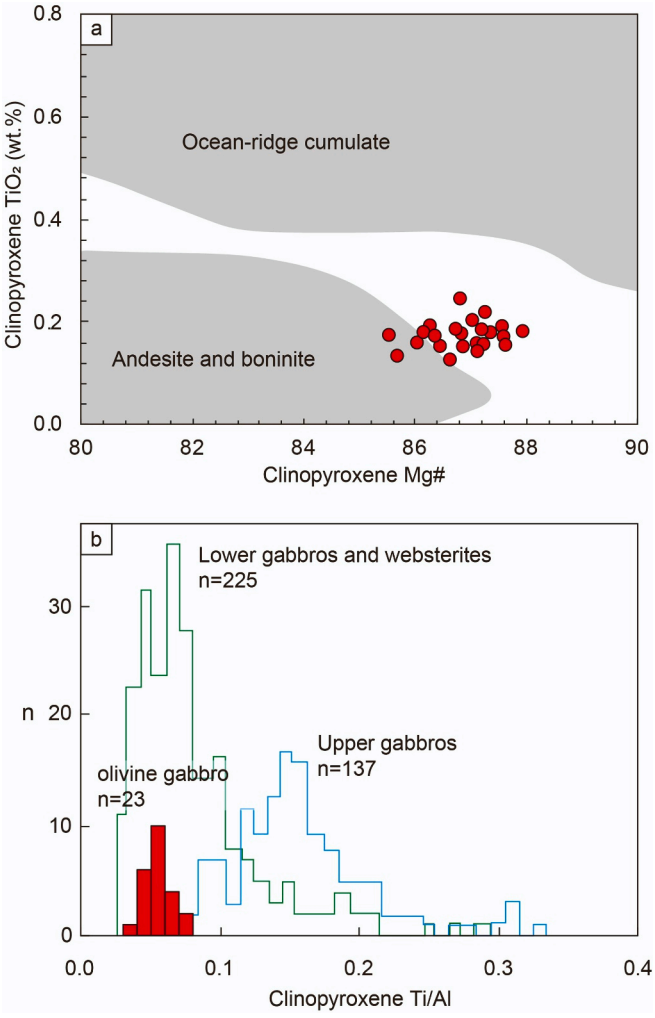

Fig. 3. (a) Mg# vs. TiO_2 of clinopyroxene. Fields of ocean ridge cumulates and Izu–Bonin arc volcanic rocks are from Nonnotte et al. (2005) and references therein. (b) and (c) Histograms of Ti/Al atomic ratios of clinopyroxene from olivine gabbros, compared to data of Thy (1987a).

Energy Dispersive Spectrometry (EDS) system connected to a JEOL JXA-8230 electron probe micro-analyzer at the Department of Earth Sciences, the University of Hong Kong. All analyses were carried out in wavelength dispersive mode with a 15 kV accelerating voltage, ~20 nA beam current, and 1 μm beam diameter with a counting time of 10–20 s. Scanning electron microscope images were obtained using a Hitachi S-3400N variable pressure scanning electron microscope (SEM) at the University of Hong Kong.

Trace elements in olivine (Sc, Ti, V, Cr, Mn, Co, Ni and Zn), clinopyroxene (Sc, Ti, V, Cr, Mn, Co, Ni and Zn), and plagioclase (K) with concentrations >1 ppm were determined by spot analysis using an Agilent 7900× inductively coupled plasma mass spectrometer (ICP-MS) coupled with a Coherent GeoLasPro 193-nm Laser Ablation (LA) system at the State Key Laboratory of Ore Deposit Geochemistry (SKLODG), Institute of Geochemistry, Chinese Academy of Sciences, Guiyang. Element abundances were calibrated using multiple reference materials (NIST610, BCR-2G, BIR-1G, BHVO-2G, and GSE-1G) with ^{29}Si as an internal standard. The reference materials ML3B-G and BCR-2G were analyzed as unknown samples to monitor the quality of the data. Off-line selection and integration of background and analytical signals, and time-drift corrections and quantitative calibration were performed using the ICPMSDataCal software of Liu et al. (2008). Repeated analyses of international glass standards ML3B-G and BCR-2G were in accordance with the referenced values within ±10%, with precisions better than

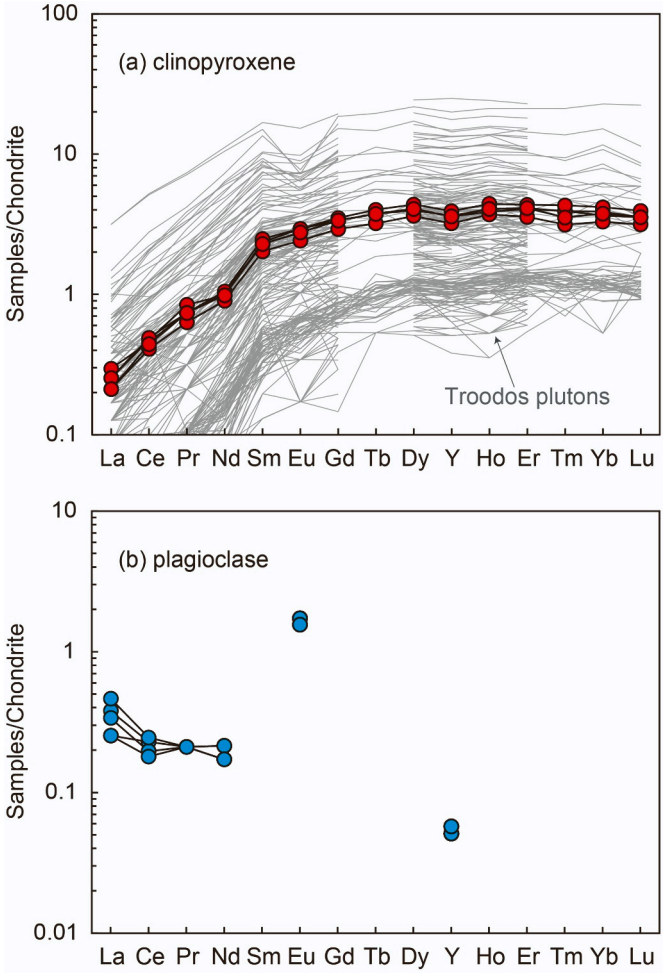

Fig. 4. Chondrite-normalized REE diagrams of clinopyroxene and plagioclase from the investigated olivine gabbros of the Troodos ophiolite. The normalization values are from Sun and McDonough (1989). Literature data for clinopyroxene in the plutons of the Troodos ophiolite are from Batanova et al. (1996), Coogan et al. (2003), and Shen et al. (2020).

10% (RSD).

Additional clinopyroxene and plagioclase grains were selected for trace element analyses at the State Key Laboratory of Nuclear Resources and Environment (SKLNRE), East China University of Technology, using a PerkinElmer NexION 1000 ICP-MS coupled to an ESL NWR-193 laser ablation system. In this round, the main focus was on trace elements with concentrations lower than 1 ppm, with special attention to REE data. All analyses were performed with a laser beam width of 80 μm, a 10 Hz pulse frequency, and a laser fluence of 5.2 J/cm^2. Each analysis comprised 20–30 s of background acquisition (gas blank) and 40 s of data acquisition. Dwell time for ^{139}La and ^{140}Ce was 80 ms, for ^{141}Pr, ^{146}Nd, ^{147}Sm, ^{153}Eu it was 60 ms, for ^{157}Gd,^{159}Tb, ^{163}Dy, ^{165}Ho, ^{166}Er, ^{169}Tm, ^{172}Yb, ^{175}Lu it was 30 ms, and for other elements it was 20 ms. Element abundances were calibrated using the Iolite software (Paton et al., 2011), with NIST612 as the external standard and ^{29}Si as the internal standard. The reference materials NIST610, NIST614, and an olivine standard MongOL Sh11–2 (Batanova et al., 2019) were analyzed in this study as unknown samples to monitor the quality of the data. Detection limits for REE calculated by the method of Longerich et al. (1996) varied from 0.01 ppm to 0.15 ppm. For the standards, NIST 610 and NIST 614, repeated analyses of most elements were in accordance with the referenced values within ±10% (Fig. S1), with precisions better than 10% (RSD). Analysis of the olivine standard MongOL Sh11–2 showed that for elements of very low concentrations (<0.1 ppm), the

Table 3
Major and trace element compositions of plagioclase of olivine gabbros in the Troodos ophiolite.

Sample No.	CY1706a1	CY1706a2	CY1706b1	CY1706b2	CY1706c
Major element (wt%)					
SiO_2	45.05	45.25	44.80	44.83	45.31
Al_2O_3	35.00	35.00	34.82	35.21	34.94
CaO	18.42	18.57	18.41	18.79	18.45
Na_2O	0.94	0.89	0.96	0.85	0.93
K_2O*	0.01	0.01	0.01	0.01	0.01
MgO*	0.04	0.08	0.11	0.04	0.09
Total	99.42	99.72	99.00	99.68	99.65
An	91.5	92.0	91.3	92.4	91.6
Ab	8.5	8.0	8.6	7.5	8.4
Or	0.1	0.1	0.1	0.1	0.1
Trace element (ppm)					
V	1.75	1.76	1.80	1.50	1.90
Sr	97.0	95.5	99.4	108	103
Y	0.08		0.08	0.08	0.09
Ba	1.86	1.99	1.91	2.27	2.04
La	0.06	0.09	0.08	0.11	0.06
Ce	0.14	0.14	0.12	0.15	0.11
Pr	0.02		0.02	0.02	0.02
Nd	0.10	0.10	0.08	0.10	0.08
Eu	0.09	0.10	0.10	0.10	0.09

* Contents of K_2O and MgO of plagioclase were determined by LA-ICP-MS

results were in accordance with the referenced values within ±20% (Fig. S1), with <30% RSD.

Linear analyses of trace elements in minerals were obtained at the SKLNRE, East China University of Technology, using a PerkinElmer NexION 1000 ICP-MS coupled to an ESL NWR-FEMTO 257 nm laser ablation system. The analyses were performed with a laser beam width of 50 μm, a 15 Hz pulse frequency, a laser fluence of 3.2 J/cm^2, and a scan velocity of 20 μm/s. The results were processed using the Iolite software (Paton et al., 2011), using the USGS glass standard, NIST612, as the primary standard.

Major and trace element mapping was performed using an Agilent 7900× ICP-MS (LA-ICP-MS) equipped with a Photon Machines Analyte HE 193-nm ArF Excimer Laser Ablation system at the In-situ Mineral Geochemistry Lab, Ore Deposit and Exploration Centre (ODEC), Hefei University of Technology, China. The Analyte HE utilizes a two-volume ablation cell designed by Laurin Technic Pty. Ablation was performed in an atmosphere of UHP He (0.9 L/min), and immediately upon exiting the cell, the aerosol was mixed with Ar (0.87 L/min) via a T-connector before entering the ICP. In addition, for high resolution profiling, the signal-smoothing device, which is used for routine analysis, was removed, providing an almost instantaneous response time. The ICP-MS system was optimized daily to maximize sensitivity for isotopes of the mass range of interest, while keeping production of molecular oxide species (i.e., ^{232}Th^{16}O/^{232}Th) as low as possible, usually <0.3%. Element maps were created by ablating sets of parallel line rasters in a grid across the sample. A beam diameter of 5 μm and a scan speed of 55 μm/s were used in this study. A laser repetition of 10 Hz was selected at a constant energy output of 40 mJ. A 20 s background acquisition was acquired at the start of scanning and, to allow for cell wash-out, gas stabilization, and computer processing, a delay of 20 s was used after ablation. The reference material NIST 610 was analyzed for data calibration at the start and end of each mapping run. Images were compiled and processed using the program LIMS (Wang et al., 2017). For each raster and every element, the average background was subtracted from its corresponding raster, and the rasters compiled into a 2-D image displaying combined background/drift corrected intensity for each element (Wang et al., 2017).

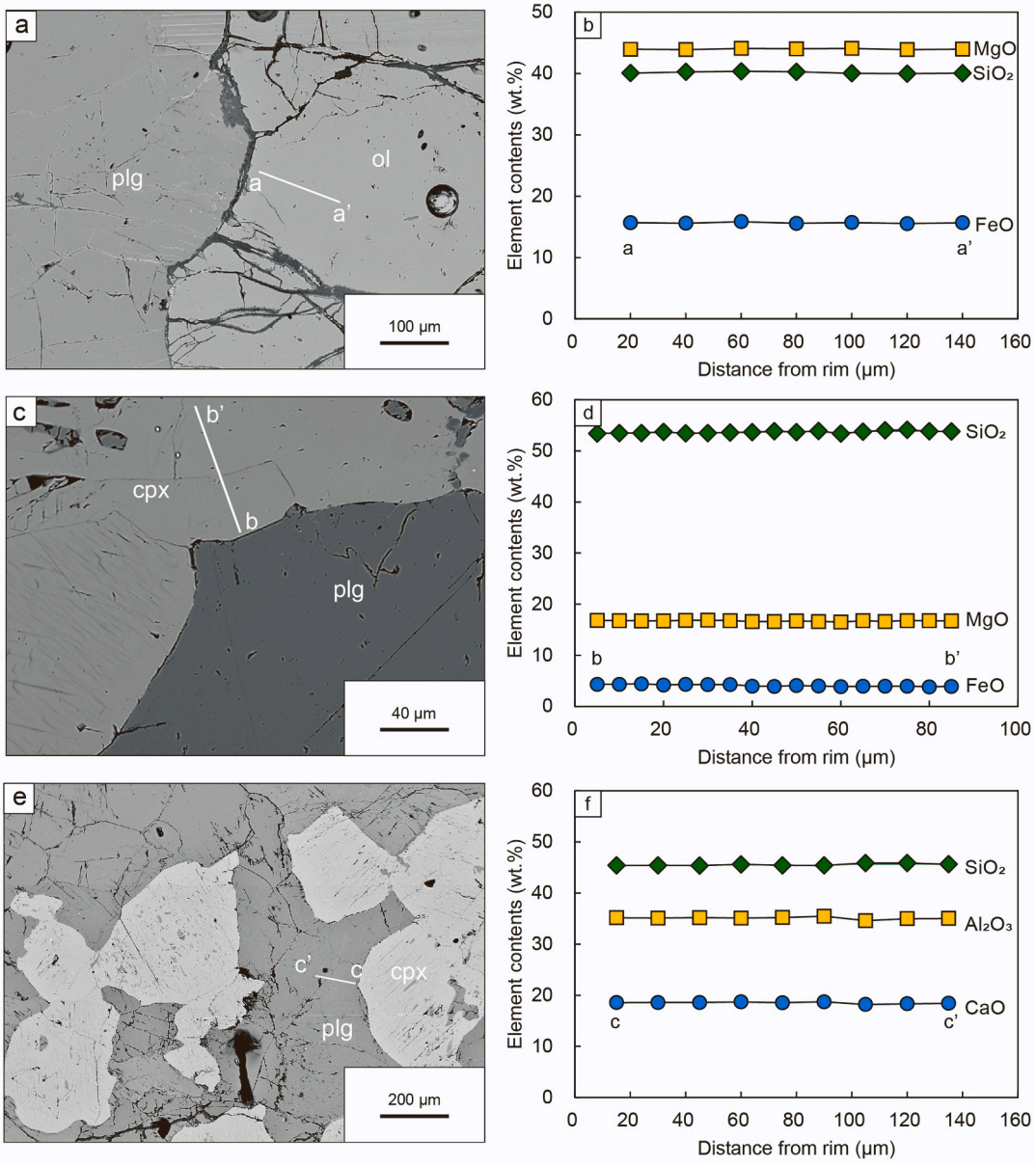

Fig. 5. Traverse analyses of major elements of minerals in the investigated olivine gabbros of the Troodos ophiolite.

5. Mineral chemistry

5.1. Olivine

Average compositions of olivine are provided in Table 1, with the complete dataset available in the Table S1 of the Supplementary File. Olivine has moderate forsterite values (Fo = atomic Mg/(Mg + Fe^{2+}) × 100) from 81.4 to 83.6. Trace element contents are 3.28–5.00 ppm for Sc, 16.9–39.0 ppm for Ti, 1.38–4.28 ppm for V, 12.0-66.4 ppm for Cr, 1681–1893 ppm for Mn, 189–203 ppm for Co, 1232–1503 ppm for Ni, and 77.9–104 for Zn.

5.2. Clinopyroxene

Average compositions of clinopyroxene are provided in Table 2, with the complete dataset available in the Table S2 and Table S3 of the Supplementary File. Mg# values (Mg# = atomic Mg/(Mg + Fe^{2+}) × 100) of clinopyroxene range from 85.5 to 87.9, slightly higher than the Fo values of olivine. The clinopyroxene is characterized by low TiO_2 contents (0.13-0.25 wt%), lower than clinopyroxene from MORB-related cumulates but similar to clinopyroxene from andesites and boninites (Fig. 3a). The low TiO_2 contents possibly indicate a low-Ti parental magma such as boninite. The Ti/Al ratios of clinopyroxene are very low (around 0.05), comparable to those of the younger gabbros and websterites in Troodos, but lower than those of the older gabbros (Fig. 3b). The clinopyroxene in our samples has higher Sc (66.2–106 ppm), Ti (759–1473 ppm), V (224–310 ppm), and Cr concentrations (1836–4273 ppm) but lower Mn (1112–1249 ppm), Co (32.6–40.6 ppm), Ni (170–230 ppm), and Zn (16.5-28.5 ppm) concentrations than olivine, which is consistent with the distribution coefficients of olivine/melt and clinopyroxene/melt (e.g., Bédard, 1994). Chondrite-normalized REE patterns of clinopyroxene display LREE depletion relative to MREE and HREE, with no clear Eu anomalies are present (Fig. 4a), indicating that the pyroxenes crystallized earlier than the plagioclase.

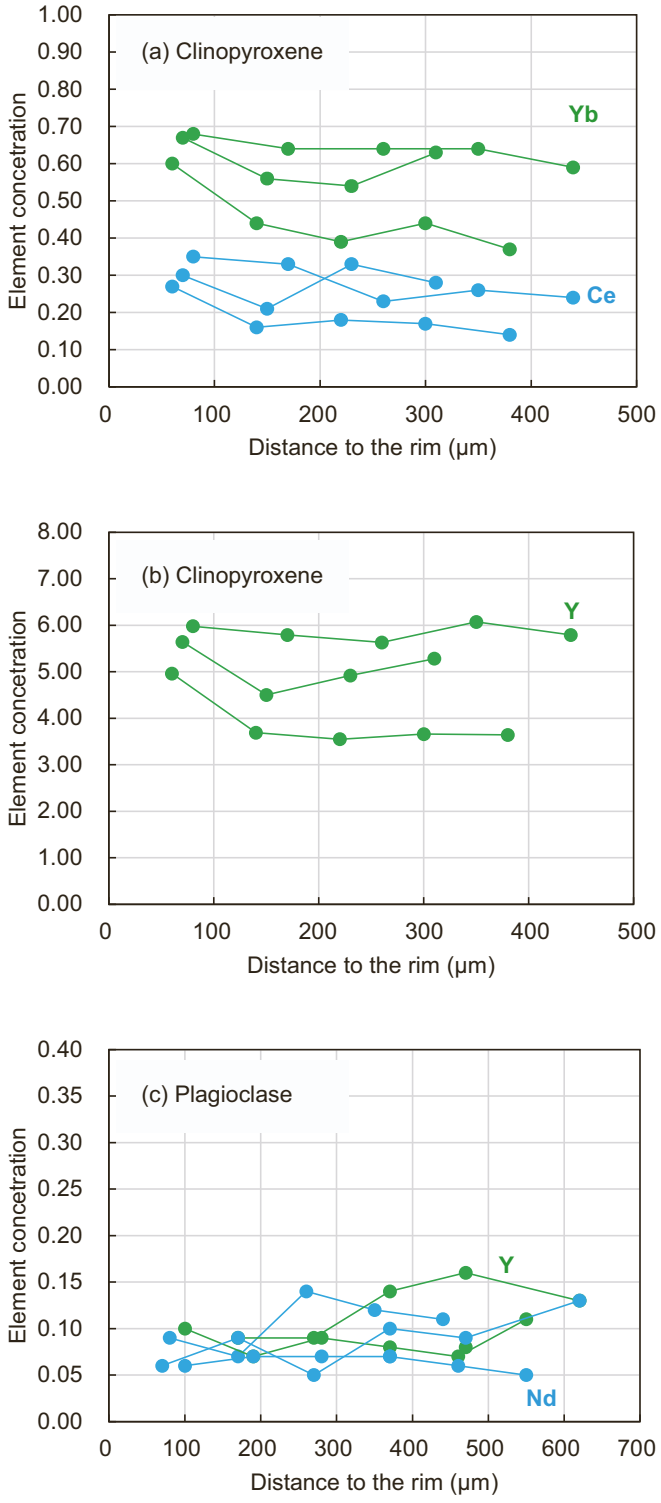

Fig. 6. Traverse analyses of trace elements of minerals in the investigated olivine gabbros of the Troodos ophiolite, determined by LA-ICP-MS (a PerkinElmer NexION 1000 ICP-MS coupled to an ESL NWR-193 laser ablation system)

5.3. Plagioclase

Average compositions of plagioclase are provided in Table 3, with a complete dataset available in the Table S4 and Table S5 of the Supplementary File. Plagioclase in the olivine gabbros has high An values (90.3-93.4), and very low REE concentrations, all of which are below the detection limits except for La, Ce, Pr, Nd, Eu, and Y. Nevertheless, the plagioclase exhibits clear LREE-enriched patterns with positive Eu anomalies (Fig. 4b).

5.4. Intra-grain chemical variations

To better understand the significance of the mineral compositions, rim-to-core traverses and element mapping were conducted for different minerals (Figs. 5-8). The data of linear analyses are given in Table S6 and Table S7 of the Supplementary File. Given that the concentrations of most trace elements in both clinopyroxene and plagioclase are very low, we mainly focus on Ce, Yb, and Y in clinopyroxene and Nd and Y in plagioclase, which have high absolute concentrations relative to other REE. All the studied grains are homogenous without any clear zonation in either major or trace elements, particularly REE (Figs. 5-8).

6. Geothermometry based on mineral equilibrium

Temperature is an important factor affecting element contents of minerals, because it not only controls their crystallization sequence (Ghiorso and Sack, 1995), but also affects the distribution coefficients of many elements (Blundy and Wood, 2003). Our petrographic observations indicate reaction between a crystal mush and a migrating magma, which led to olivine dissolution and crystallization of clinopyroxene, and subsequent crystallization of plagioclase from evolved intergranular melts within the framework of olivine and clinopyroxene (Fig. 2). The interaction of a migrating interstitial liquid with a pre-existing crystal mush has been well documented in oceanic gabbros and is known as "reactive porous flow" (Lissenberg et al., 2013; Lissenberg and Dick, 2008; Lissenberg and MacLeod, 2016; Sanfilippo et al., 2020). Through this process, major and trace element zonation in minerals commonly develops as a result of diffusion and disequilibrium during magma-mineral reaction. However, all the minerals in this study have constant intra-grain compositions without any clear zonation (Figs. 5–8), and it seems very likely that the chemical compositions of the clinopyroxene and the plagioclase have reached equilibrium with the migrating magma, even though these minerals did not crystallize at the same time.

Based on the assumption of mineral equilibrium, the clinopyroxene-plagioclase REE thermometer developed by Sun and Liang (2017) was used to obtain the equilibrium temperature. The results for the olivine gabbros are between 1282 °C and 1317 °C (Fig. 9a). All the REE and Y except Eu plot on a linear trend of (B/100) versus ln(D)-A in the diagram generated by the clinopyroxene-plagioclase REE thermometer (Fig. 9b), which further support that equilibrium of these elements between clinopyroxene and plagioclase was achieved and not disrupted later.. Using the clinopyroxene-plagioclase Mg thermometer of Sun and Lissenberg (2018), lower temperatures were obtained (930 °C to 1047 °C) (Fig. 9a). The differences between these two thermometers are due to the different diffusion rates of REE and Mg (Sun and Liang, 2017; Sun and Lissenberg, 2018). Specifically, REE have very slow diffusion rates in both plagioclase and clinopyroxene and their distribution preferentially records crystallization, or near-crystallization, temperatures of the rock (Cherniak, 2003; Sun and Liang, 2017; Van Orman et al., 2001), whereas Mg has a fast diffusion rate, and its distribution is readily reset during further cooling of the minerals (Müller et al., 2013; Faak et al., 2014; Van Orman et al., 2014). As illustrated in Sun and Lissenberg (2018), the combination of these two thermometers allows calculation of the cooling rate of the gabbros. Using the code of Sun and Lissenberg (2018), we suggest that the olivine gabbros studied here experienced rapid cooling (−2 °C/year log units) (Fig. 9c).

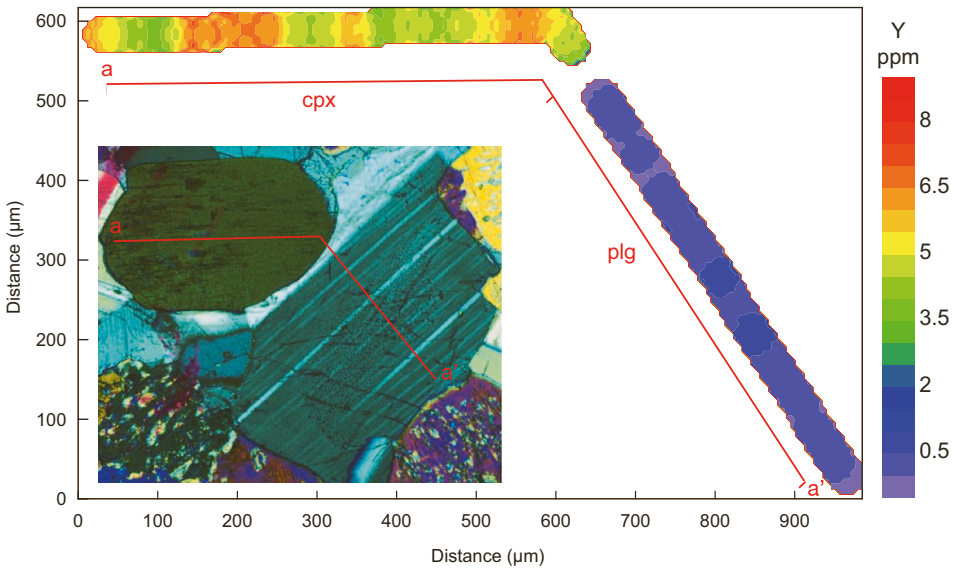

Fig. 7. A compositional profile of Y from clinopyroxene to plagioclase in an analyzed olivine gabbro of the Troodos ophiolite, determined by LA-ICP-MS (a PerkinElmer NexION 1000 ICP-MS coupled to an ESL NWR-FEMTO 257nm laser ablation system).

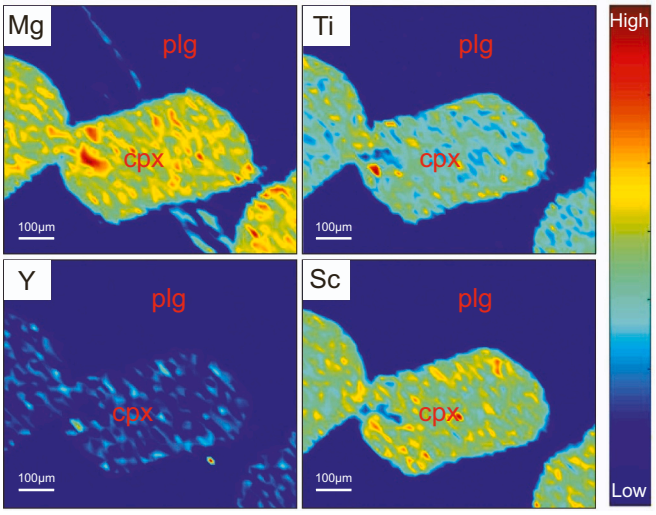

Fig. 8. Major and trace element mapping of minerals in the investigated olivine gabbros of the Troodos ophiolite.

7. Discussion

7.1. Nature of the parental magma of the olivine gabbros

Major element concentrations of minerals are important indicators of the composition of their parental magmas. For Troodos gabbroic rocks, Thy (1987a) used Ti/Al ratios of clinopyroxene to distinguish the parental magmas of the gabbros and volcanic rocks. Specifically, in borehole CY-4, clinopyroxene in the uppermost, older gabbro has very low Ti/Al ratios (average = 0.16) similar to clinopyroxene in the LPL (average = 0.13), whereas clinopyroxenes in the younger gabbros at greater depths in the borehole have very low Ti/Al (average = 0.09) similar to clinopyroxene in the UPL (average = 0.06) (Thy, 1987a). In the present study, clinopyroxene in the olivine gabbros sampled in the lower pluton has consistently low Ti/Al (around 0.05), indicating that these gabbros are most likely related to the boninites of the UPL.

As mentioned above, the UPL in the Troodos ophiolites consists of two groups of boninites, i.e., the Group-A boninites that occur mainly along the ophiolite's northern flank and the Group-B boninites that occur along the Arakapas valley and its western and eastern extensions. The question that arises is thus, "to which group of boninites in the UPL are the olivine gabbros analyzed in this study related?" We use trace element compositions of clinopyroxene in the gabbros to address this problem. Given that clinopyroxene and plagioclase are homogeneous, and that both were likely in equilibrium with the migrating interstitial magma, it should be possible to determine their parental magma composition by back-calculating their trace elements using appropriate distribution coefficients. However, to date, distribution coefficients between clinopyroxene and boninitic magmas are rarely studied, and complicated by the fact that water contents in the magmas can greatly affect the distribution coefficients (McDade et al., 2003). Instead, we attempt to constrain the composition of the parental magma using direct comparison with natural clinopyroxenes of similar compositions, whose parental magmas have been well documented. Clinopyroxene phenocrysts from the Troodos Upper Lavas sampled by Sobolev et al. (1996) have almost the same trace element compositions as clinopyroxenes of the olivine gabbros in this study (Fig. 10a). Moreover, the chemical compositions of melt inclusions in these volcanic clinopyroxenes are close to boninite and show flat trace element patterns, similar to those of Group-A but different from Group-B boninites (Fig. 10b). This suggests that the olivine gabbros in this study were most likely derived from percolation of Group A boninite-related liquids, and not those of the Group B 'infill lavas'. This conclusion is also supported by the phase assemblage of the olivine gabbros. From petrographic observations, the crystallization sequence of these rocks is olivine-clinopyroxene-plagioclase, consistent with that of Group-A boninites (olivine-clinopyroxene-plagioclase) but different from that of Group-B boninites (olivine-orthopyroxene-clinopyroxene-plagioclase) (Thy and Xenophontos, 1991).

7.2. Implications for the Troodos ophiolite

The Olympus (Axis) Sequence of the Troodos ophiolite is considered to have formed at a spreading ridge with low magma supply, partly because the plutonic sequence is made up of two different series of small discrete plutons. This is different from the situation envisaged for fast-spreading ridges with copious magma (Malpas, 1990), such as the Oman ophiolite that has a more continuous plutonic sequence. The rapid cooling rate documented by the olivine gabbros in the present study is consistent with slow-spreading ridges (e.g., Coogan et al., 2007; Zhang

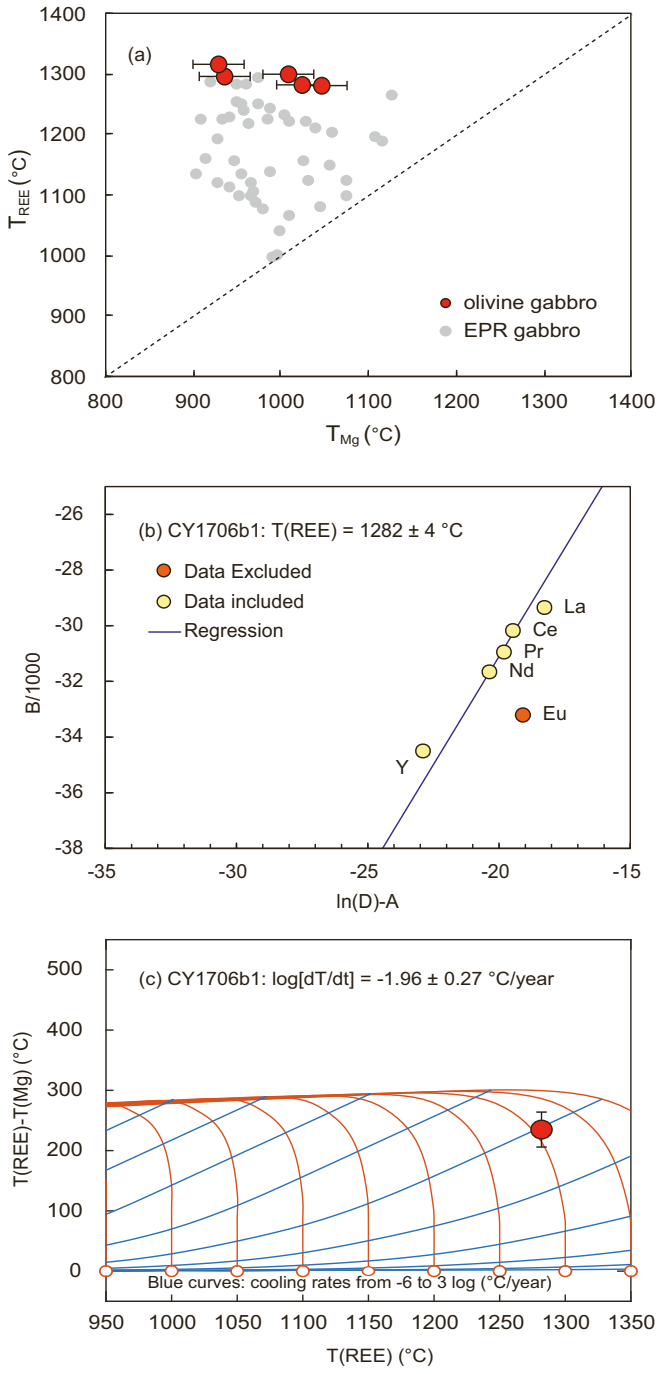

Fig. 9. (a) Mg bulk closure temperature (T_{Mg}) vs. REE bulk closure temperature (T_{REE}).. Data of the fast-spreading East Pacific Rise (EPR) at Hess Deep is from Sun and Lissenberg (2018). (b) The representative (B/100) vs (ln(D)-A) plot, generated by the clinopyroxene-plagioclase REE thermometer developed by Sun and Liang (2017), suggesting that clinopyroxene and plagioclase have reached REE equilibration. (c) The cooling rate of a representative olivine gabbro sample calculated using the code of Sun and Lissenberg (2018).

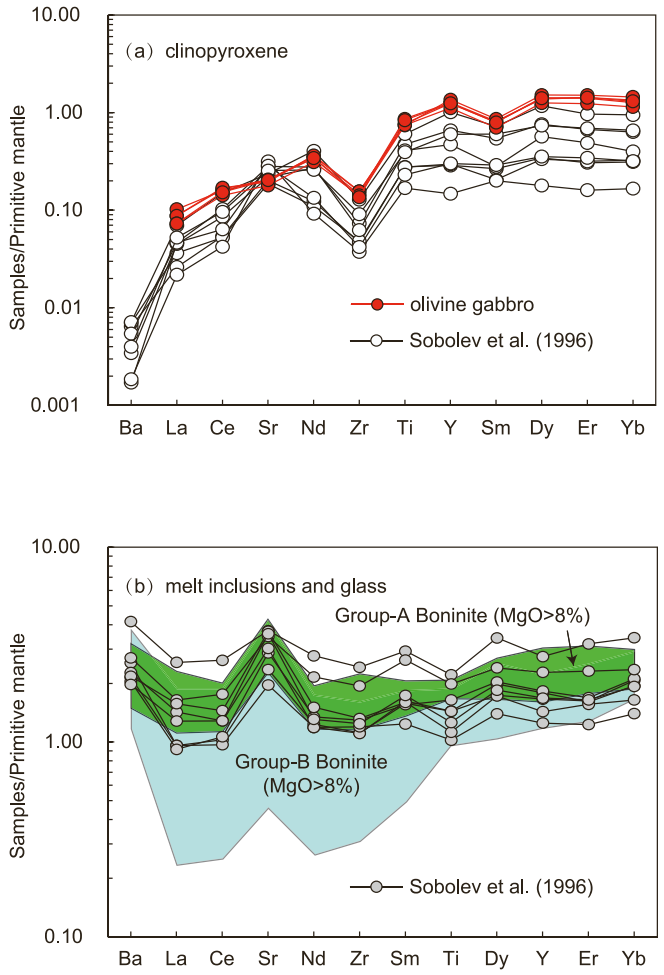

Fig. 10. (a) Trace element compositions of clinopyroxenes in the investigated olivine gabbros of the Troodos ophiolite, compared to those of clinopyroxene phenocrysts in the UPL (Sobolev et al., 1996). (b) Trace element compositions of melt inclusions in the clinopyroxene phenocrysts of Sobolev et al. (1996), compared those of boninitic glasses in the Troodos ophiolite (Golowin et al., 2017; Osozawa et al., 2012; Pearce and Robinson, 2010; Woelki et al., 2018, 2019, and 2020).

et al., 2020), and can be explained by efficient heat removal due to crustal-scale hydrothermal circulation (Sun and Lissenberg, 2018; VanTongeren et al., 2008) or emplacement of plutons into thick and cool lithosphere (Coogan et al., 2007).

Olivine gabbros in this study display petrographic features indicative of reactive porous flow, in which a migrating magma reacted with a pre-existing crystal mush (Lissenberg et al., 2013; Lissenberg and Dick, 2008; Lissenberg and MacLeod, 2016). Unlike oceanic gabbros, which show significant major and trace element zonation in minerals after reaction with migrating magmas (e.g., Lissenberg et al., 2013; Lissenberg and MacLeod, 2016), all the minerals in this study exhibit relatively constant compositions without any clear zonation (Figs. 5–8). In addition, REE concentrations in the clinopyroxene and plagioclase are in equilibrium at high temperatures and have not been disrupted by later processes (Fig. 9a). Consequently, these minerals are thought to have reached equilibrium with the interstitial migrating magma. On the other hand, because the inferred composition of the magma is similar to that of Group-A boninites, it is very likely that some erupted Group-A boninites might have been modified by melt-mineral reaction in the lower crust and consequently may not accurately represent their primary magma compositions (Lissenberg et al., 2013; Lissenberg and Dick, 2008; Lissenberg and MacLeod, 2016).

In order to further evaluate the effects of melt-rock reaction on the lavas, Group-A boninitic glasses of the Troodos ophiolite are displayed in Mg# vs. major oxide diagrams (Fig. 11). We first model crystallization of the Troodos primary boninite by using the software alphaMELTS (Smith and Asimow, 2005). The composition of the Troodos primary boninite is from Hu et al. (2021). The modelling pressure is 0.2 GPa and the water content of the parental boninite is set to either 2 wt% or 4 wt% after Woelki et al. (2020). For most major element oxides except CaO, e.

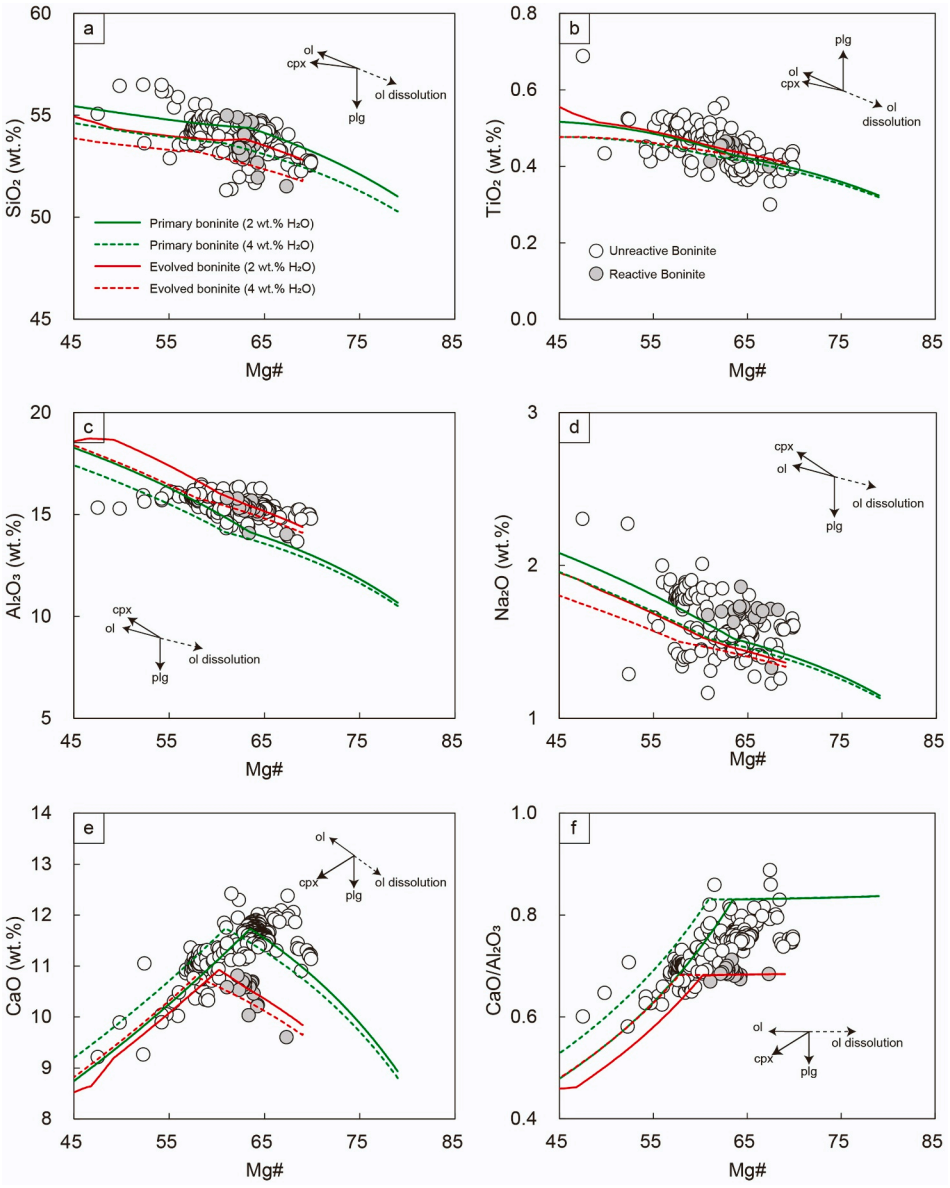

Fig. 11. Major element compositions of the Group-A boninites in the Troodos ophiolite. Magma crystallization was simulated by using the software alphaMELTS (Smith and Asimow, 2005). The modelling pressure is 0.2 GPa. The starting composition of the primary boninite and the evolved boninite were based on melt inclusions in high-Fo olivine phenocrysts from Hu et al. (2021) and glass CY130 from Osozawa et al. (2012), respectively. The water content of the primary boninite is set to 2 wt% and 4 wt%, respectively, after Woelki et al. (2020).

g., SiO_2, TiO_2, Al_2O_3, and Na_2O, the trends due to crystallization of olivine and clinopyroxene are quite similar. Therefore, their trends in the simple crystallization process (olivine-clinopyroxene) and the reactive porous flow process (i.e., olivine dissolution together with crystallization of clinopyroxene and then plagioclase) are nearly opposite, and cannot efficiently distinguish these two processes (Fig. 11a–d).

In contrast, crystallization of olivine and clinopyroxene each change the CaO contents of the magma in a different way, and a reactive porous flow process in which olivine is dissolved can be easily distinguished from a crystallization process in the Mg#-CaO and Mg#-CaO/Al_2O_3 diagrams (Fig. 11e and f). It is clear that, some boninites ("reactive boninite" in Fig. 11) have higher Mg# values at given CaO contents and higher CaO/Al_2O_3 ratios than others ("unreactive boninite" in Fig. 11), indicative of olivine dissolution during reactive porous flow.

However, the CaO and CaO/Al_2O_3 compositional features of the "reactive boninite" could be alternatively explained by crystallization of a magma which has lower CaO concentrations than the parental magma of the "unreactive boninite" (Fig. 11). If so, the parental magma of the "reactive boninite" could have been derived either from a source different from that of the parental magma of the "unreactive boninite", or the parental magma of the "reactive boninite" evolved from the parental magma of the "unreactive boninite" following processes such as crustal assimilation or magma mixing. In either case, the "reactive boninite" should have different trace element compositions from the "unreactive boninite". In contrast, a reactive porous flow process involving olivine dissolution would not significantly affect most trace elements such as REE and HFSE, because olivine is extremely depleted in these elements. In Fig. 12, the two groups of boninites share the same trace element compositions, therefore the major element variation more likely reflects reactive porous flow in the lower crust. It is therefore proposed that, some boninites in the Troodos ophiolite might have experienced melt-rock reaction during their ascent through the lower oceanic crust. Thus, attempts to identify the primary magma compositions by using such rocks should be approached with caution.

8. Conclusions

Olivine gabbros in the lower parts of the plutonic sequence of the Troodos ophiolite, exhibit typical orthocumulate textures with clear evidence of interaction between a crystal mush and a migrating interstitial melt. However, all the minerals show relatively constant compositions without any clear zonation, suggesting the migrating melt and

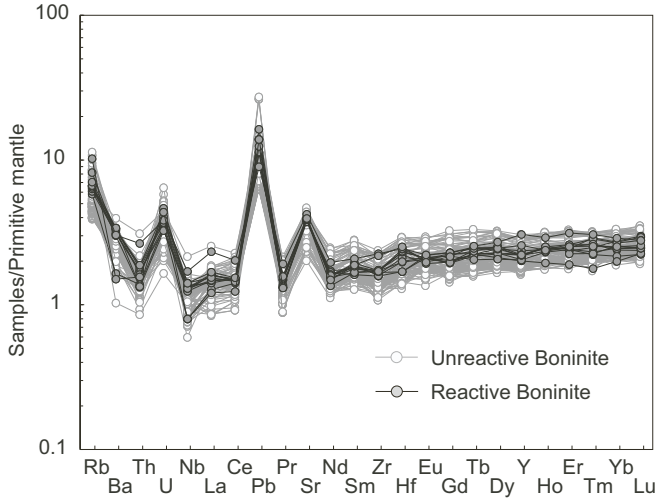

Fig. 12. Primitive mantle normalized trace element patterns of the Group-A boninites in the Troodos ophiolite. The normalization values are from Sun and McDonough (1989). Data source is the same as that of Fig. 11. The consistent trace element compositions of reactive and unreactive boninites support the hypothesis of porous reactive flow, in which olivine dissolution had a limited effect on the trace element compositions of the magma.

the minerals had reached equilibrium. Using a clinopyroxene-plagioclase REE geothermometer, clinopyroxene and plagioclase in the olivine gabbros equilibrated at temperatures of around 1300 °C. Based on trace element compositions of the clinopyroxene, we suggest that the migrating interstitial magma was genetically related to the boninites in the ophiolite. A compilation of data shows that some boninitic lavas have been affected by melt-rock reaction in the lower oceanic crust.

Declaration of Competing Interest

The authors declare that they have no known competing financial interests or personal relationships that could have appeared to influence the work reported in this paper.

Acknowledgements

We are grateful for constructive comments by Dr. Jaroslav Dostal, an anonymous reviewer and the Editor, Prof. Paul T. Robinson that greatly improved the quality of the manuscript. Drs. Wu Yadong and Bai Zhong-Jie are thanked for their helpful discussion on the earliest version of the paper. Drs. Fangyue Wang, Yan Zhao, and Shaohao Zou are sincerely thanked for their kind help on LA-ICP-MS analysis. This study was supported by the National Natural Science Foundation of China (91962216).

Appendix A. Supplementary data

Supplementary data to this article can be found online at https://doi.org/10.1016/j.lithos.2022.106759.

References

Abelson, M., Baer, G., Agnon, A., 2001. Evidence from gabbro of the Troodos ophiolite for lateral magma transport along a slow-spreading mid-ocean ridge. Nature 409 (6816), 72–75.
Barnes, S.J., 1986. The effect of trapped liquid crystallization on cumulus mineral compositions in layered intrusions. Contrib. Mineral. Petrol. 93 (4), 524–531.
Batanova, V.G., Sobolev, A.V., Schmincke, H.U., 1996. Parental melts of the intrusive cumulates of the Troodos massif, Cyprus: a study of clinopyroxenes and melt inclusions in plagioclase. Petrology 4 (3), 255–264.
Batanova, V.G., Thompson, J.M., Danyushevsky, L.V., Portnyagin, M.V., Garbe-Schönberg, D., Hauri, E., Kimura, J.I., Chang, Q., Senda, R., Goemann, K., Chauvel, C., Campillo, S., Ionov, D., Sobolev, A.V., 2019. New olivine reference material for in situ microanalysis. Geostand. Geoanal. Res. 43 (3), 453–473.
Bédard, J.H., 1994. A procedure for calculating the equilibrium distribution of trace elements among the minerals of cumulate rocks, and the concentration of trace elements in the coexisting liquids. Chem. Geol. 118 (1–4), 143–153.
Blundy, J., Wood, B., 2003. Partitioning of trace elements between crystals and melts. Earth Planet. Sci. Lett. 210 (3–4), 383–397.
Borghini, G., Rampone, E., 2007. Postcumulus processes in oceanic-type olivine-rich cumulates: the role of trapped melt crystallization versus melt/rock interaction. Contrib. Mineral. Petrol. 154 (6), 619–633.
Bowen, N.L., 1928. The Evolution of the Igneous Rocks. Dover Publ, New York.
Cameron, W.E., 1985. Petrology and origin of primitive lavas from the Troodos ophiolite, Cyprus. Contrib. Mineral. Petrol. 89, 239–255.
Chen, Y., Niu, Y., Shen, F., Gao, Y., Wang, X., 2020. New U-Pb zircon age and petrogenesis of the plagiogranite, Troodos ophiolite, Cyprus. Lithos 362, 105472.
Cherniak, D.J., 2003. REE diffusion in feldspar. Chem. Geol. 193 (1–2), 25–41.
Coogan, L.A., 2014. 4.14 - The lower Oceanic Crust. In: Holland, H.D., Turekian, K.K. (Eds.), Treatise on Geochemistry (Second Edition). Elsevier, Oxford, pp. 497–541.
Coogan, L.A., Saunders, A.D., Kempton, P.D., Norry, M.J., 2000. Evidence from oceanic gabbros for porous melt migration within a crystal mush beneath the Mid-Atlantic Ridge. Geochem. Geophys. Geosyst. 1 (9).
Coogan, L., Banks, G., Gillis, K., MacLeod, C., Pearce, J., 2003. Hidden melting signatures recorded in the Troodos ophiolite plutonic suite: evidence for widespread generation of depleted melts and intra-crustal melt aggregation. Contrib. Mineral. Petrol. 144 (4), 484–506.
Coogan, L.A., Jenkin, G.R.T., Wilson, R.N., 2007. Contrasting cooling rates in the lower oceanic crust at fast-and slow-spreading ridges revealed by geospeedometry. J. Petrol. 48 (11), 2211–2231.
Edwards, S., Hudson-Edwards, K.A., Cann, J., Malpas, J., Xenophontos, C., 2010. Cyprus, Vol. 7. Terra Publishing.
Faak, K., Coogan, L.A., Chakraborty, S., 2014. A new Mg-in-plagioclase geospeedometer for the determination of cooling rates of mafic rocks. Geochim. Cosmochim. Acta 140, 691–707.
Gao, Y., Hoefs, J., Hellebrand, E., von der Handt, A., Snow, J.E., 2007. Trace element zoning in pyroxenes from ODP Hole 735B gabbros: diffusive exchange or synkinematic crystal fractionation? Contrib. Mineral. Petrol. 153 (4), 429–442.
Gass, I.G., MacLeod, C.J., Murton, B.J., Panayiotou, A., Simonian, K.O., Xenophontos, C., 1994. The Geological Evolution of the Southern Troodos Transform Fault Zone (No. 9). Geological Survey Department.
Geological Survey Department Cyprus, 1995. Geological Map of Cyprus: Nicosia, Cyprus, Ministry of Agriculture, Natural Resources and Environment, Government of Cyprus, scale, 1, p. 250,000.
Ghiorso, M.S., Sack, R.O., 1995. Chemical mass transfer in magmatic processes IV. A revised and internally consistent thermodynamic model for the interpolation and extrapolation of liquid-solid equilibria in magmatic systems at elevated temperatures and pressures. Contrib. Mineral. Petrol. 119 (2), 197–212.
Gibson, I.L., Malpas, J., Robinson, P.T., Xenophontos, C., 1989. Cyprus crustal study project: initial report. Hole CY-4.
Godel, B., Barnes, S.J., Maier, W.D., 2011. Parental magma composition inferred from trace element in cumulus and intercumulus silicate minerals: an example from the lower and lower critical zones of the Bushveld complex, South-Africa. Lithos 125 (1–2), 537–552.
Golowin, R., Portnyagin, M., Hoernle, K., Sobolev, A., Kuzmin, D., Werner, R., 2017. The role and conditions of second-stage mantle melting in the generation of low-Ti tholeiites and boninites: the case of the Manihiki Plateau and the Troodos ophiolite. Contrib. Mineral. Petrol. 172 (11), 1–18.
Hu, W.J., Zhou, M.F., Malpas, J., Ren, Z.Y., 2021. High-Ca boninitic melt inclusions in lavas of the Troodos ophiolite and a reappraisal of genetic relationships between different lava types. GSA. Bulletin. 133 (9–10), 1831–1850.
Ishizuka, O., Tani, K., Reagan, M.K., 2014. Izu-Bonin-Mariana forearc crust as a modern ophiolite analogue. Elements 10, 115–120.
Lee, C.T.A., Harbert, A., Leeman, W.P., 2007. Extension of lattice strain theory to mineral/mineral rare-earth element partitioning: an approach for assessing disequilibrium and developing internally consistent partition coefficients between olivine, orthopyroxene, clinopyroxene and basaltic melt. Geochim. Cosmochim. Acta 71 (2), 481–496.
Lissenberg, C.J., Dick, H.J., 2008. Melt–rock reaction in the lower oceanic crust and its implications for the genesis of mid-ocean ridge basalt. Earth Planet. Sci. Lett. 271 (1–4), 311–325.
Lissenberg, C.J., MacLeod, C.J., 2016. A reactive porous flow control on mid-ocean ridge magmatic evolution. J. Petrol. 57 (11−12), 2195–2220.
Lissenberg, C.J., MacLeod, C.J., Howard, K.A., Godard, M., 2013. Pervasive reactive melt migration through fast-spreading lower oceanic crust (Hess Deep, equatorial Pacific Ocean). Earth Planet. Sci. Lett. 361, 436–447.
Liu, Y., Hu, Z., Gao, S., Günther, D., Xu, J., Gao, C., Chen, H., 2008. In situ analysis of major and trace elements of anhydrous minerals by LA-ICP-MS without applying an internal standard. Chem. Geol. 257, 34–43.
Liu, T., Wu, F.Y., Liu, C.Z., Tribuzio, R., Ji, W.B., Zhang, C., Xu, Y., Zhang, W.Q., 2018. Variably evolved gabbroic intrusions within the Xigaze ophiolite (Tibet): new insights into the origin of ophiolite diversity. Contrib. Mineral. Petrol. 173 (11), 1–21.
Liu, T., Dick, H.J., Liu, C.Z., Wu, F.Y., Ji, W.B., Zhang, C., Zhang, W.Q., Zhang, Z.Y., Lin, Y.Z., Zhang, Z., 2021. Tectonic controls on block rotation and sheeted sill emplacement in the Xigaze Ophiolite (Tibet): the construction mode of slow-spreading and ultraslow-spreading oceanic crusts. Geochem. Geophys. Geosyst. 22 (3), e2020GC009297.

Longerich, H.P., Jackson, S.E., Günther, D., 1996. Inter-laboratory note. Laser ablation inductively coupled plasma mass spectrometric transient signal data acquisition and analyte concentration calculation. J. Anal. At. Spectrom. 11 (9), 899–904.
Malpas, J., 1990. Crustal accretionary processes in the Troodos ophiolite, Cyprus: evidence from field mapping and deep crustal drilling. In: Troodos 1987. Symposium, pp. 65–74.
Malpas, J., Brace, T., Dunsworth, S.M., 1989. Structural and petrologic relationships of the CY-4 Drill Hole of the Cyprus Crustal Study Project. In: Ottawa, O.N. (Ed.), Cyprus Crustal Study Project; Initial Report, Hole CY-4. Canada, Geological Survey of, Canada, pp. 39–67.
Marchesi, C., Garrido, C.J., Godard, M., Belley, F., Ferré, E., 2009. Migration and accumulation of ultra-depleted subduction-related melts in the Massif du Sud ophiolite (New Caledonia). Chem. Geol. 266 (3–4), 171–186.
McDade, P., Blundy, J.D., Wood, B.J., 2003. Trace element partitioning between mantle wedge peridotite and hydrous MgO-rich melt. Am. Mineral. 88 (11–12), 1825–1831.
Mehegan, J.M., 1988. Temporal, Spatial and Chemical Evolution of the Troodos Ophiolite, Cyprus: Supra-Subduction Zone Volcanism in the Tethyan Sea (Doctoral Dissertation, PhD thesis, Dalhousie University, Halifax).
Miyashiro, A., 1973. The Troodos ophiolitic complex was probably formed in an island arc. Earth Planet. Sci. Lett. 19, 218–224.
Mukasa, S.B., Ludden, J.N., 1987. Uranium-lead isotopic ages of plagiogranites from the Troodos ophiolite, Cyprus, and their tectonic significance. Geology 15, 825–828.
Müller, T., Dohmen, R., Becker, H.W., Ter Heege, J.H., Chakraborty, S., 2013. Fe–Mg interdiffusion rates in clinopyroxene: experimental data and implications for Fe–Mg exchange geothermometers. Contrib. Mineral. 166, 1563–1576.
Niu, Y., Gilmore, T., Mackie, S., Greig, A., Bach, W., 2002. Mineral chemistry, whole-rock compositions, and petrogenesis of Leg 176 gabbros: data and discussion. In: Proceedings of the Ocean Drilling Program, Scientific Results, vol. 176. Ocean Drilling Program, College Station, TX, pp. 1–60.
Nonnotte, P., Ceuleneer, G., Benoit, M., 2005. Genesis of andesitic–boninitic magmas at mid-ocean ridges by melting of hydrated peridotites: geochemical evidence from DSDP Site 334 gabbronorites. Earth Planet. Sci. Lett. 236 (3–4), 632–653.
Osozawa, S., Shinjo, R., Lo, C.H., Jahn, B.M., Hoang, N., Sasaki, M., Wakabayashi, J., 2012. Geochemistry and geochronology of the Troodos ophiolite: an SSZ ophiolite generated by subduction initiation and an extended episode of ridge subduction? Lithosphere 4, 497–510.
Paton, C., Hellstrom, J., Paul, B., Woodhead, J., Hergt, J., 2011. Iolite: Freeware for the visualisation and processing of mass spectrometric data. J. Anal. At. Spectrom. https://doi.org/10.1039/c1ja10172b.
Pearce, J.A., Robinson, P.T., 2010. The Troodos ophiolitic complex probably formed in a subduction initiation, slab edge setting. Gondwana Res. 18, 60–81.
Pearce, J.A., Lippard, S.J., Roberts, S., 1984. Characteristics and tectonic significance of supra-subduction zone ophiolites. Geol. Soc. Lond., Spec. Publ. 16, 77–94.
Rampone, E., Borghini, G., Godard, M., Ildefonse, B., Crispini, L., Fumagalli, P., 2016. Melt/rock reaction at oceanic peridotite/gabbro transition as revealed by trace element chemistry of olivine. Geochim. Cosmochim. Acta 190, 309–331.
Regelous, M., Haase, K.M., Freund, S., Keith, M., Weinzierl, C.G., Beier, C., Brandl, P.A., Schmidt, H., 2014. Formation of the Troodos Ophiolite at a triple junction: evidence from trace elements in volcanic glass. Chem. Geol. 386, 66–79.
Robertson, A., Xenophontos, C., 1993. Development of concepts concerning the Troodos ophiolite and adjacent units in Cyprus. Geol. Soc. Lond., Spec. Publ. 76, 85–119.
Robinson, P.T., Melson, W.G., O'Hearn, T., Schmincke, H.U., 1983. Volcanic glass compositions of the Troodos ophiolite, Cyprus. Geology 11 (7), 400–404.
Sanfilippo, A., Tribuzio, R., 2013. Building of the deepest crust at a fossil slow-spreading Centre (Pineto gabbroic sequence, Alpine Jurassic ophiolites). Contrib. Mineral. Petrol. 165 (4), 705–721.
Sanfilippo, A., MacLeod, C.J., Tribuzio, R., Lissenberg, C.J., Zanetti, A., 2020. Early-stage melt-rock reaction in a cooling crystal mush beneath a slow-spreading mid-ocean ridge (IODP Hole U1473A, Atlantis Bank, Southwest Indian Ridge). Front. Earth Sci. 473.
Shen, F., Niu, Y., Chen, Y., Gao, Y., Wang, X., Duan, M., Shan, L., 2020. Origin of magmatic harzburgite as a result of boninite magma evolution–an illustration using layered harzburgite-dunite cumulate from the Troodos ophiolite complex. Lithos 376, 105764.
Simonian, K.T., Gass, I.G., 1978. Arakapas fault belt, Cyprus: A fossil transform fault. Geol. Soc. Am. Bull. 89, 1220–1230.
Sinton, J.M., Detrick, R.S., 1992. Mid-ocean ridge magma chambers. J. Geophys. Res. Solid Earth 97 (B1), 197–216.
Smith, P.M., Asimow, P.D., 2005. Adiabat_1ph: a new public front-end to the MELTS, pMELTS, and pHMELTS models. Geochem. Geophys. Geosyst. 6 (2).
Sobolev, A.V., Migdisov, A.A., Portnyagin, M.V., 1996. Incompatible element partitioning between clinopyroxene and basalt liquid revealed by the study of melt inclusions in minerals from Troodos lavas, Cyprus. Petrology 4 (3), 307–317.
Stern, R.J., Reagan, M., Ishizuka, O., Ohara, Y., Whattam, S., 2012. To understand subduction initiation, study forearc crust: to understand forearc crust, study ophiolites. Lithosphere 4, 469–483.
Sun, C., Liang, Y., 2014. An assessment of subsolidus re-equilibration on REE distribution among mantle minerals olivine, orthopyroxene, clinopyroxene, and garnet in peridotites. Chem. Geol. 372, 80–91.
Sun, C., Liang, Y., 2017. A REE-in-plagioclase–clinopyroxene thermometer for crustal rocks. Contrib. Mineral. Petrol. 172 (4), 24.
Sun, C., Lissenberg, C.J., 2018. Formation of fast-spreading lower oceanic crust as revealed by a new Mg–REE coupled geospeedometer. Earth Planet. Sci. Lett. 487, 165–178.
Sun, S.S., McDonough, W.F., 1989. Chemical and isotopic systematics of oceanic basalts: implications for mantle composition and processes. Geol. Soc. Lond., Spec. Publ. 42 (1), 313–345.
Thy, P., 1987a. Magmas and magma chamber evolution, Troodos ophiolite, Cyprus. Geology 15 (4), 316–319.
Thy, P., 1987b. Petrogenetic implications of mineral crystallization trends of Troodos cumulates, Cyprus. Geol. Mag. 124 (1), 1–11.
Thy, P., Xenophontos, C., 1991. Crystallization orders and phase chemistry of glassy lavas from the pillow sequences, Troodos ophiolite, Cyprus. J. Petrol. 32 (2), 403–428.
Van Orman, J.A., Grove, T.L., Shimizu, N., 2001. Rare earth element diffusion in diopside: influence of temperature, pressure, and ionic radius, and an elastic model for diffusion in silicates. Contrib. Mineral. Petrol. 141 (6), 687–703.
Van Orman, J.A., Cherniak, D.J., Kita, N.T., 2014. Magnesium diffusion in plagioclase: Dependence on composition, and implications for thermal resetting of the 26Al–26Mg early solar system chronometer. Earth Planet. Sci. Lett. 385, 79–88.
VanTongeren, J.A., Kelemen, P.B., Hanghøj, K., 2008. Cooling rates in the lower crust of the Oman ophiolite: ca in olivine, revisited. Earth Planet. Sci. Lett. 267 (1–2), 69–82.
Wager, L.R., Brown, G.M., 1968. Layered Igneous Rocks. Oliver and Boyd, London.
Wang, F., Ge, C., Ning, S., Nie, L., Zhong, G., White, N., 2017. A new approach to LA-ICP-MS mapping and application in geology. Acta Petrol. Sin. 33, 3422–3436 (in Chinese with English abstract).
Wang, P., Zhao, G., Liu, Q., Han, Y., Zhang, Y., Yao, J., Yu, S., 2021. Slab-controlled progressive evolution of the Kudi back-arc ophiolite in response to the rollback of the Proto-Tethys oceanic slab, in Western Kunlun, NW Tibetan Plateau. Lithos 380, 105877.
Whattam, S.A., Stern, R.J., 2011. The 'subduction initiation rule': a key for linking ophiolites, intra-oceanic forearcs, and subduction initiation. Contrib. Mineral. Petrol. 162, 1031–1045.
White, W.M., 2013. Geochemistry. John Wiley and Sons, Chichester.
White, W.M., Klein, E.M., 2014. 4.13-Composition of the oceanic crust. In: Holland, H.D., Turekian, K.K. (Eds.), Treatise on Geochemistry (Second Edition). Elsevier, Oxford, pp. 457–496.
Woelki, D., Regelous, M., Haase, K.M., Romer, R.H., Beier, C., 2018. Petrogenesis of boninitic lavas from the Troodos Ophiolite, and comparison with Izu–Bonin–Mariana fore-arc crust. Earth Planet. Sci. Lett. 498, 203–214.
Woelki, D., Regelous, M., Haase, K.M., Beier, C., 2019. Geochemical mapping of a paleo-subduction zone beneath the Troodos Ophiolite. Chem. Geol. 523, 1–8.
Woelki, D., Michael, P., Regelous, M., Haase, K., 2020. Enrichment of H2O and fluid-soluble trace elements in the Troodos Ophiolite: evidence for a near-trench origin. Lithos 356, 105299.
Yamasaki, T., Maeda, J., Mizuta, T., 2006. Geochemical evidence in clinopyroxenes from gabbroic sequence for two distinct magmatisms in the Oman ophiolite. Earth Planet. Sci. Lett. 251 (1–2), 52–65.
Yang, S.H., Maier, W.D., Godel, B., Barnes, S.J., Hanski, E., O'Brien, H., 2019. Parental magma composition of the Main Zone of the Bushveld complex: evidence from in situ LA-ICP-MS trace element analysis of silicate minerals in the cumulate rocks. J. Petrol. 60 (2), 359–392.
Zhang, W.Q., Liu, C.Z., Dick, H.J., 2020. Evidence for multi-stage melt transport in the lower ocean crust: the Atlantis bank gabbroic massif (IODP Hole U1473A, SW Indian Ridge). J. Petrol. 61 (9), egaa082.